NOTE

Mannosylated Cationic Liposomes/CpG DNA Complex for the Treatment of Hepatic Metastasis after Intravenous Administration in Mice

YUKARI KURAMOTO, SHIGERU KAWAKAMI, SHUWEN ZHOU, KYOUICHI FUKUDA, FUMIYOSHI YAMASHITA, MITSURU HASHIDA

Department of Drug Delivery Research, Graduate School of Pharmaceutical Sciences, Kyoto University, Sakyo-ku, Kyoto 606-8501, Japan

Received 19 November 2007; accepted 19 May 2008

Published online 11 July 2008 in Wiley InterScience (www.interscience.wiley.com). DOI 10.1002/jps.21475

ABSTRACT: Immunotherapy using immunostimulatory CpG DNA could be a promising new therapeutic approach to combat refractory hepatic metastasis. In this study, we report the use of a conventional cationic liposomes/CpG DNA complex (Bare/CpG DNA lipoplex) and a mannosylated cationic liposomes/CpG DNA complex (Man/CpG DNA lipoplex) for effective inhibition of hepatic metastasis in mice. After intravenous administration of Bare/CpG DNA lipoplex, higher amounts of IL-12 and IFN-γ were produced in serum or liver compared with naked CpG DNA, and their production was increased further by Man/CpG DNA lipoplex. Then, Bare/CpG DNA lipoplex and Man/CpG DNA lipoplex were administered intravenously to hepatic metastasis model mice, and the numbers of tumor cells (colon26/Luc) were quantitatively assayed. The number of tumor cells in Man/CpG DNA lipoplex-treated mice was same as those in Bare/CpG DNA lipoplex-treated mice. These results suggest that intravenous administration of not only Bare/CpG DNA lipoplex but also Man/CpG DNA lipoplex could be an efficient immunotherapy for hepatic metastasis. © 2008 Wiley-Liss, Inc. and the American Pharmacists Association J Pharm Sci 98:1193–1197, 2009

Keywords: cancer; gene delivery; gene therapy; liposomes; non-viral gene delivery

INTRODUCTION

Hepatic metastasis is a common event in the course of gastrointestinal malignancies. Although postoperative therapy is needed for hepatic metastasis, conventional chemotherapy has not proven effective in improving long-term results.[1] CpG DNA, about 30-base oligonucleotides containing CpG dinucleotides, which is derived from the bacterial DNA, is recognized by Toll-like receptors (TLR)-9 expressed by macrophages.[2] Macrophages treated with CpG DNA induce Th1 type antitumor cytokines, such as interleukin (IL)-12, which, in turn, stimulate the production of interferon (IFN)-γ by natural killer cells.[3] There are many resident macrophages, Kupffer cells, in the liver; therefore, delivery of CpG DNA into Kupffer cells and induction of Th1 type cytokines would effectively inhibit hepatic metastasis. However, little naked CpG DNA is thought to distribute in the liver Kupffer cells after intravenous administration, since the molecular weight of naked CpG DNA is about 8,000.

Correspondence to: Mitsuru Hashida (Telephone: +81-75-753-4525; Fax: +81-75-753-4575; E-mail: hashidam@pharm.kyoto-u.ac.jp)

Journal of Pharmaceutical Sciences, Vol. 98, 1193–1197 (2009)

As for the Kupffer cell-selective delivery of oligonucleotide, receptor-mediated uptake is a promising approach because these cells express high levels of mannose receptors.[4] Recently, we developed Man-liposomes that are efficiently taken up by macrophages via mannose receptor-mediated endocytosis. We have also developed a Kupffer cell-specific nuclear factor (NF)-κB decoy transfer system by Man-liposomes.[5] These observations prompted us to investigate whether targeted Kupffer cell delivery could be achieved by a Man-liposomes/CpG DNA complex (Man/CpG DNA lipoplex). This is our initial report of Man/CpG DNA lipoplex for the systemic delivery of CpG DNA for treatment of hepatic metastasis. Naked CpG DNA and a conventional cationic liposomes/CpG DNA complex (Bare/CpG DNA lipoplex) were used as controls.

MATERIALS AND METHODS

Animals

Male Balb/c (6-week-old) mice and female ICR (4-week-old) mice were purchased from the Shizuoka Agricultural Cooperative Association for Laboratory Animals (Shizuoka, Japan). All the animals were housed with free access to food and water. The light (dark/light cycle was 2/12 h), temperature, and humidity were constantly maintained throughout the experiments. All animal experiments were approved by the Animal Experimentation Committee of the Graduate School of Pharmaceutical Sciences, Kyoto University.

Preparation of Liposomes and Their Complex with CpG DNA

Man-liposomes and Bare-liposomes were prepared as reported previously.[6] Stock liposome solutions and phosphorothioate CpG DNA (5′-TCGACGTT-TTGACGTTTTGACGTTTT-3′, Operon Biotechnologies, Inc., Tokyo, Japan) in 5% dextrose were mixed at a charge ratio of 1.0:3.1 (−/+), to obtain the Man/CpG DNA lipoplex and the Bare/CpG DNA lipoplex. The mean particle size and ζ-potential of the lipoplexes were measured by Zetasizer nano ZS equipment (Malvern Instruments Ltd, Worchestershire, UK).

Statistical Analysis

Statistical comparisons were performed by one-way ANOVA for multiple groups. Post hoc multiple comparisons were made by using Tukey's test.

RESULTS AND DISCUSSION

To investigate the physicochemical properties of Man/CpG DNA lipoplex and Bare/CpG DNA lipoplex, their particle sizes and ζ-potential were evaluated. The mean particle sizes of the Man/CpG DNA lipoplex and Bare/CpG DNA lipoplex were 120.0 ± 1.2 nm and 110.6 ± 0.7 nm, respectively, and both lipoplexes showed similar and monomodal distribution pattern (Fig. 1). The ζ-potential of the Man/CpG DNA lipoplex and the Bare/CpG DNA lipoplex were 57.8 ± 0.8 mV and 53.0 ± 0.2 mV, respectively ($n = 3$).

After intravenous administration of naked CpG DNA, the serum IL-12 concentration was about 200 pg/mL and IFN-γ was near the limit of detection at 4 h. These observations of naked CpG DNA agree with the report by Whitmore et al.[7] We previously demonstrated that intravenously administered CpG motif containing plasmid DNA complexed with cationic liposomes composed of DOTMA/cholesterol efficiently pro-

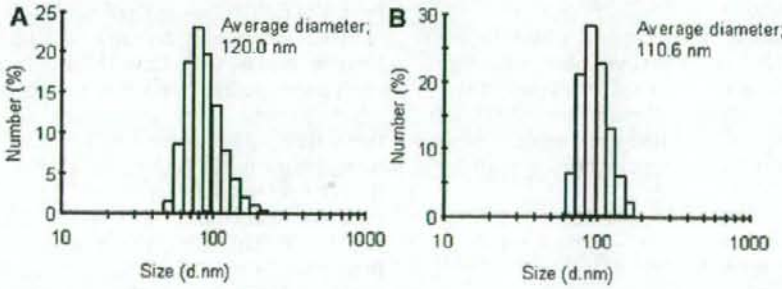

Figure 1. Particle size distribution of (A) Man/CpG DNA lipoplex and (B) Bare/CpG DNA lipoplex.

DOI 10.1002/jps

duced IL-12 and IFN-γ.[8] Therefore, DOTMA/cholesterol liposomes were selected for delivery of CpG DNA. As shown in Figure 2, when Bare/CpG DNA lipoplex was administered, the levels of IL-12 and, in particular, IFN-γ in serum increased compared with naked CpG DNA. Moreover, when Man/CpG DNA lipoplex was administered, the level of both IL-12 and IFN-γ in serum was significantly increased compared with Bare/CpG DNA lipoplex (Fig. 2). IL-12 and IFN-γ were not detected at 4 h after intravenous administration of unloaded Bare-liposomes (4 mg total lipid/kg) or Man-liposomes (3 mg total lipid/kg). This phenomenon is corresponding to the recent report by Shin et al. that little IFN-γ was detected in serum at 6 h after intravenous administration of unloaded cationic liposomes (20 mg total lipid/kg).[9] Similarly, the hepatic concentration of IFN-γ was increased by naked CpG DNA, Bare/CpG DNA lipoplex, and Man/CpG DNA lipoplex, in that order (Fig. 3). Previously, we have shown that cultured mouse peritoneal macrophages treated with Bare/GpC DNA-lipoplex, which had no CpG motifs, did not induce any TNF-α production.[10] Taking these into considerations, CpG DNA delivered by Bare- and Man-liposomes could effectively induce the production of Th1 type cytokines in serum and liver after intravenous administration.

The antitumor effects of intravenously administered Bare/CpG DNA lipoplex and Man/CpG DNA lipoplex in the hepatic metastasis model were analyzed using colon26/Luc cells, a murine colorectal adenocarcinoma cell line that stably expresses firefly luciferase gene.[11] The numbers of tumor cells were quantitatively evaluated by measuring the luciferase activity in the liver. As shown in Figure 4, the number of tumor cells in Man/CpG DNA lipoplex- and Bare/CpG DNA lipoplex-treated mice was about 10% compared with that of naked CpG DNA. As far as the antitumor effect of CpG DNA is concerned, Whitmore et al.[7] demonstrated that antitumor effect was correlated with serum Th1 cytokine levels using pulmonary metastasis model. Moreover, Yano et al.[12] also reported that in hepatic metastasis model, intravenously administered cationic liposome/scrambled siRNA complex hardly inhibited the tumor growth in the liver. These observations suggest that cationic liposome/nucleic acid complex did not directly inhibit the hepatic metastasis. The number of tumor cells in naked CpG DNA-treated mice was unexpectedly significantly different from that in

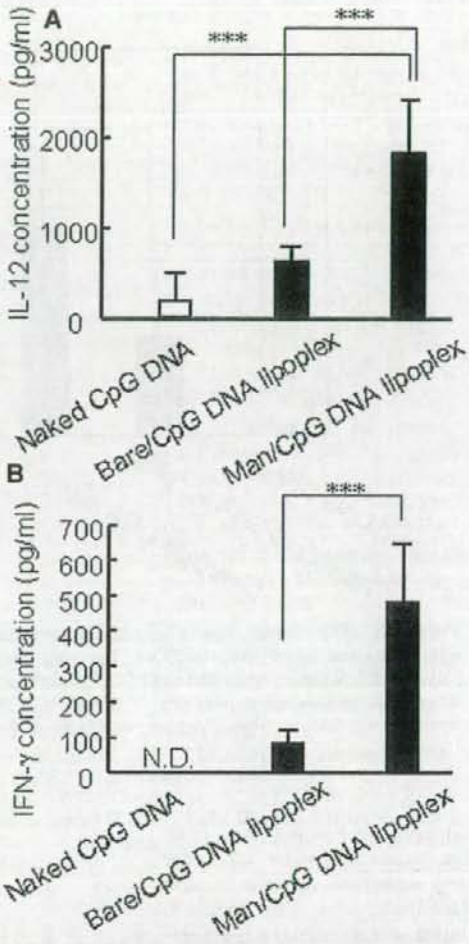

Figure 2. IL-12 and IFN-γ concentration in serum after intravenous administration of Man/CpG DNA lipoplex, Bare/CpG DNA lipoplex, and naked CpG DNA. The concentrations of IL-12 (A) and IFN-γ (B) in serum at 4 h after intravenous administration of Man/CpG DNA lipoplex, Bare/CpG DNA lipoplex, naked CpG DNA (10 μg DNA/mouse), were measured by ELISA kits (eBioscience, Inc., San Diego, CA). IL-12 and IFN-γ were not detected at 4 h after intravenous administration of unloaded Bare-liposomes (4 mg total lipid/kg) or Man-liposomes (3 mg total lipid/kg; data not shown). The lipid doses of unloaded Bare-liposomes and Man-liposomes were based on the amount of component in a 10 μg DNA dose of lipoplex/mouse; thus about 4 mg total lipid/kg for unloaded Bare-liposomes and about 3 mg total lipid/kg for unloaded Man-liposomes were utilized. Results are expressed as mean + SD ($n \geq 5$). ***$p < 0.001$; N.D., not detected.

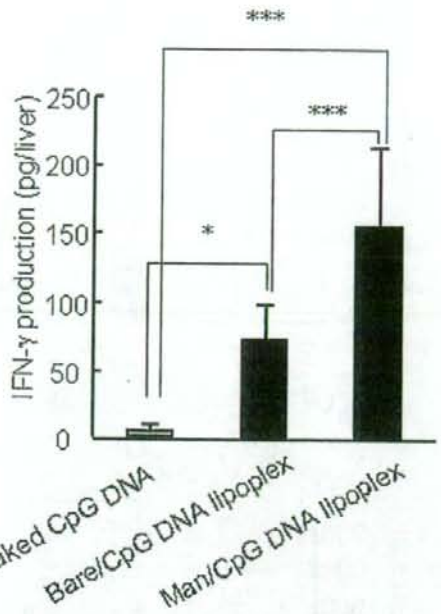

Figure 3. IFN-γ production in liver after intravenous administration of Man/CpG DNA lipoplex, Bare/CpG DNA lipoplex, and naked CpG DNA. Four hours after intravenous administration of Man/CpG DNA lipoplex, Bare/CpG DNA lipoplex, and naked CpG DNA (10 μg DNA/mouse), mice were sacrificed, then the blood in the liver was removed by intraportal injection of 5 mL saline. The concentration of IFN-γ in the liver were measured by ELISA kit (R & D Systems, Inc., Minneapolis, MN) as previously described.[15] Results are expressed as mean + SD ($n = 6$). $^{*}p < 0.05$; $^{***}p < 0.001$.

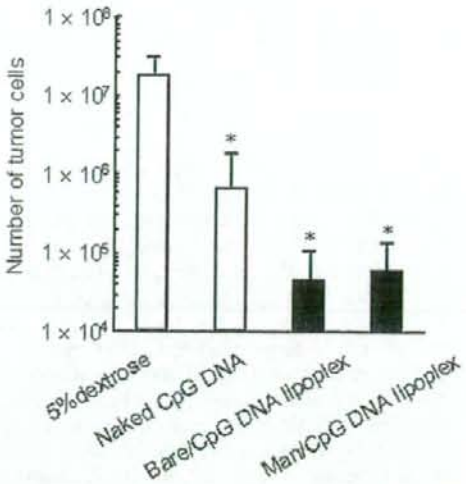

Figure 4. The number of tumor cells in the liver of the hepatic metastasis mice after intravenous administration of Man/CpG DNA lipoplex, Bare/CpG DNA lipoplex, and naked CpG DNA. Colon26 cells that stably express the firefly luciferase gene (colon26/Luc)[11] were inoculated intraportally into male Balb/c mice (1×10^5 cells/mouse). Three days later, 5% dextrose, Man/CpG DNA lipoplex, Bare/CpG DNA lipoplex, and naked CpG DNA (10 μg DNA/mouse) were administered to the tail vein of the mice. Ten days after tumor inoculation, the luciferase activity of the livers was measured and converted to the number of colon26/Luc cells as previously reported.[10] Results are expressed as mean + SD ($n \geq 5$). $^{*}p < 0.05$; the number of tumor cells was significantly different from 5% dextrose-treated group.

control (5% dextrose-treated) mice (Fig. 4). This result might be supported by the result that naked CpG DNA slightly induced IL-12 in serum (Fig. 2). Taking these into considerations, intravenously administered CpG DNA complexed with Man- and/or Bare-liposomes could effectively inhibit hepatic metastasis with Th1 cytokine production.

Intravenous administration of Bare/CpG DNA lipoplex moderately induced IL-12 and IFN-γ production, to inhibit hepatic metastasis as well as Man/CpG DNA lipoplex. These observations about Bare/CpG DNA lipoplex might partly corresponding to our previous report that intravenously administered Bare-liposomes/plasmid DNA complex,[13] and NF-κB decoy oligonucleotides[14] is taken up by the liver non-parenchymal cells mainly via Kupffer cell phagocytosis. Since intravenous administration of Bare-liposomes/plasmid DNA, which contains CpG motifs, produce IL-12, IFN-γ, and TNF-α in serum after taken up by the liver Kupffer cells,[15] Bare-liposomes are an effective carrier to deliver CpG DNA to Kupffer cells.

Immunosuppression is one of the most serious issues raised by systemic chemotherapy using conventional anti-cancer drugs. Recently, it was reported that CpG DNA reversed the reduction in NK cell activity and Th1 type cytokine production by chemotherapeutic agents,[16] and retarded the growth of solid tumors.[17] Therefore, combination of chemotherapy and immunotherapy is expected to enhance the therapeutic effect against hepatic metastasis by reversing the immunosuppressed state. These observations lead us to believe that chemotherapeutic agents and Man/CpG DNA lipoplex will be a promis-

DOI 10.1002/jps

ing combination therapy to combat hepatic metastasis.

In conclusion, intravenously administered Man/CpG DNA lipoplex and/or Bare/CpG DNA lipoplex inhibit hepatic metastasis by the production of IL-12 and IFN-γ. Although further investigations are needed to clarify the molecular mechanisms operating in this system, this information will be valuable for the development of immunotherapy to combat refractory hepatic metastasis.

ACKNOWLEDGMENTS

This work was supported in part by Grants-in-Aid for Scientific Research from Ministry of Education, Culture, Sports, Science, and Technology of Japan, by Health and Labour Sciences Research Grants for Research on Advanced Medical Technology from the Ministry of Health, Labour and Welfare of Japan, by the Mochida Memorial Foundation for Medical and Pharmaceutical Research, and by the 21st Century COE Program "Knowledge Information Infrastructure for Genome Science."

REFERENCES

1. Liu XL, Zhang WH, Jiang HC. 2003. Current treatment for liver metastasis from colorectal cancer. World J Gastroenterol 9:193–200.
2. Krieg AM, Yi AK, Matson S, Waldschmidt TJ, Bishop GA, Teasdale R, Koretzky GA, Klinman DM. 1995. CpG motifs in bacterial DNA trigger direct B-cell activation. Nature 374:546–549.
3. Chace JH, Hooker NA, Mildenstein KL, Krieg AM, Cowdery JS. 1997. Bacterial DNA-induced NK cell IFN-γ production is dependent on macrophage secretion of IL-12. Clin Immunol Immunopathol 84:185–193.
4. Kuiper J, Brower A, Knook DL, Berkel TJC. 1994. Kupffer and sinusoidal endothelial cells. In: Arias IM, Boyar JL, Fausto N, Jakoby WB, Schachter DA, Shafritz DA, editors. The liver: biology and pathobiology, 3rd edition. New York: Raven Press, Ltd. pp 791–818.
5. Higuchi Y, Kawakami S, Oka M, Yabe Y, Yamashita F, Hashida M. 2006. Intravenous administration of mannosylated cationic liposomes/NFkappaB decoy complexes effectively prevent LPS-induced cytokine production in a murine liver failure model. FEBS Lett 580:3706–3714.
6. Kawakami S, Sato A, Nishikawa M, Yamashita F, Hashida M. 2000. Mannose receptor-mediated gene transfer into macrophages using novel mannosylated cationic liposomes. Gene Ther 7:292–299.
7. Whitmore MM, Li S, Falo L, Jr., Huang L. 2001. Systemic administration of LPD prepared with CpG oligonucleotides inhibits the growth of established pulmonary metastases by stimulating innate and acquired antitumor immune responses. Cancer Immunol Immunother 50:503–514.
8. Kawakami S, Ito Y, Charoensit P, Yamashita F, Hashida M. 2006. Evaluation of proinflammatory cytokine production induced by linear and branched polyethylenimine/plasmid DNA complexes in mice. J Pharmacol Exp Ther 317:1382–1390.
9. Shin D, Kim SI, Park M, Kim M. 2007. Immunostimulatory properties and antiviral activity of modified HBV-specific siRNAs. Biochem Biophys Res Commun 364:436–442.
10. Kuramoto Y, Kawakami S, Zhou S, Fukuda K, Yamashita F, Hashida M. 2008. Efficient peritoneal dissemination treatment obtained by an immunostimulatory phosphorothioate-type CpG DNA/cationic liposome complex in mice. J Control Release 126:274–280.
11. Kuramoto Y, Nishikawa M, Hyoudou K, Yamashita F, Hashida M. 2006. Inhibition of peritoneal dissemination of tumor cells by single dosing of phosphodiester CpG oligonucleotide/cationic liposome complex. J Control Release 115:226–233.
12. Yano J, Hirabayashi K, Nakagawa S, Yamaguchi T, Nogawa M, Kashimori I, Naito H, Kitagawa H, Ishiyama K, Ohgi T, Irimura T. 2004. Antitumor activity of small interfering RNA/cationic liposome complex in mouse models of cancer. Clin Cancer Res 10:7721–7726.
13. Mahato RI, Kawabata K, Nomura T, Takakura Y, Hashida M. 1995. Physicochemical and pharmacokinetic characteristics of plasmid DNA/cationic liposome complexes. J Pharm Sci 84:1267–1271.
14. Higuchi Y, Kawakami S, Oka M, Hashida M. 2006. Suppression of TNFα production in LPS induced liver failure in mice after intravenous administration of cationic liposome/NFκB decoy complex. Pharmazie 61:144–147.
15. Sakurai F, Terada T, Yasuda K, Yamashita F, Takakura Y, Hashida M. 2002. The role of tissue macrophages in the induction of proinflammatory cytokine production following intravenous injection of lipoplexes. Gene Ther 9:1120–1126.
16. Wang XS, Sheng Z, Ruan YB, Guang Y, Yang ML. 2005. CpG oligodeoxynucleotides inhibit tumor growth and reverse the immunosuppression caused by the therapy with 5-fluorouracil in murine hepatoma. World J Gastroenterol 11:220–224.
17. Balsari A, Tortoreto M, Besusso D, Petrangolini G, Sfondrini L, Maggi R, Ménard S, Pratesi G. 2004. Combination of a CpG-oligodeoxynucleotide and a topoisomerase I inhibitor in the therapy of human tumour xenografts. Eur J Cancer 40:1275–1281.

Magnetic targeting after femoral artery administration and biocompatibility assessment of superparamagnetic iron oxide nanoparticles

Hui-Li Ma,[1] Xian-Rong Qi,[1] Wu-Xiao Ding,[1] Yoshie Maitani,[2] Tsuneji Nagai[2]
[1]*Department of Pharmaceutics, School of Pharmaceutical Sciences, Peking University, Beijing 100083, China*
[2]*Institute of Medicinal Chemistry, Hoshi University, Shinagawa-Ku, Tokyo 142-850, Japan*

Received 14 October 2006; revised 22 December 2006; accepted 30 January 2007
Published online 6 July 2007 in Wiley InterScience (www.interscience.wiley.com). DOI: 10.1002/jbm.a.31346

Abstract: Ferrofluids are attractive candidates for magnetic targeting system because of their fluidity and magnetism. The magnetic nanoparticles in ferrofluids should have combined properties of superparamagnetic behavior, target localization, and biocompatibility. The magnetic targeting and biocompatibility of superparamagnetic iron oxide nanoparticles stabilized by alginate (SPION-alginate) was investigated *in vitro* and *in vivo*. The localization of SPION-alginate by an external magnetic field *in vitro* was quantitatively evaluated by determining the iron content, and the results revealed that the localization ratio of SPION-alginate was 56%. Magnetic targeting of the SPION-alginate after femoral artery administration with the magnetic field in rats was quantitatively investigated by iron content and qualitatively confirmed by histological evaluation and magnetic resonance imaging. The ratio of iron content between the target site and the nontarget site were 8.88 at 0.5 h and 7.50 at 2 h, respectively. The viability of RAW264.7 cells and L929 cells was apparently unaltered upon exposure to SPION-alginate. The incubation with erythrocytes indicated that the SPION-alginate did not induce erythrocytes hemolysis and aggregation. In conclusions, the SPION-alginate had magnetic targeting with an external magnetic field and did not be detained at the injection site without the magnetic field. The SPION-alginate was generally considered to be biocompatible in cytotoxicity and hemolysis aspects. © 2007 Wiley Periodicals, Inc. J Biomed Mater Res 84A: 598–606, 2008

Key words: superparamagnetic iron oxide nanoparticles (SPION); magnetic targeting; biocompatibility; alginate; localization ratio

INTRODUCTION

Drug targeting always attracts the most interests from pharmaceutical researchers, among which magnetic drug targeting has been widely studied for the advantages to reduce the amount of drug needed and to reduce the adverse effect of drug. In magnetic targeting, a magnetic compound was injected into the systemic circulation, and then stopped with a powerful magnetic field in the target site.[1] Compared with other targeting vectors, such as ligand-targeting particulates and enzyme-triggered drug release system, magnetic targeting system is feasible to produce, reliable to control and can be specifically modified for drug delivery applications. Current applications of magnetic targeting system include magnetic delivery of chemotherapy drugs to tumors,[2–4] magnetic targeting of radioisotope,[1,5] magnetic hyperthermia,[6] magnetically enhanced gene therapy,[7] and magnetic embolization.[8] Some successes are achieved, but the results from both laboratory and clinical trials are far from satisfactory. Currently, one of the main problems is that the localization effect of magnetic carrier in target site with the magnetic field is not as good as expected.

Many factors, including physio-chemical properties of magnetic carrier, target sites, magnetic field, and the route of administration, can affect the magnetic targeting effect. When addressing the physiochemical properties of magnetic carrier, we have to consider the size, magnetization and matrix materials. Magnetic carriers can be grouped into ferrofluids, magnetic nanospheres, and magnetic microspheres according to the size from 10 nm to 100 μm. Ferrofluids are stable colloidal systems that com-

Correspondence to: X.R. Qi; e-mail: qixr2001@yahoo.com.cn
Contract grant sponsor: National High Technology Research and Development Program of China; contract grant number: 863 Program, No. 2003AA326020

posed of solid, magnetic, single-domain magnetic nanoparticles, typically between 3 and 15 nm in diameter, in a nonmagnetic solvent.[9] Because of the fluidity and magnetism of ferrofluids, they have been widely used in the magnetic targeting system. For biomedical applications, it is required that the magnetic nanoparticles should have combined properties of superparamagnetic behavior, high magnetic saturation, good stability, target localization ability, and biocompatibility. In our laboratory, a kind of ferrofluids, superparamagnetic iron oxide nanoparticles stabilized by alginate (SPION-alginate), was prepared successfully. They were composed of iron oxide (Fe_3O_4) with 5–10 nm core diameter and had good magnetic susceptibility.[10]

The magnetic field should be of sufficient strength to attract the magnetic particles into the desired area or target site. The higher magnetic flux density and magnetic gradient it is, the better the location effect is.[2] Because of the superparamagnetism and liquid state of ferrofluids, the magnetism of ferrofluids was usually weaker than that of magnetic microsphere. Therefore, a higher magnetic field is needed to attract or hold the injected ferrofluids to the target site.

The route of administration and target site can also greatly affect the magnetic targeting effect. If the target site is a part of reticuloendothelial system (RES), such as liver or spleen, most of magnetic carriers always accumulate in it by the passive targeting effect through intravenous injection. If the target site is a tumor outside RES, the passive accumulation in RES becomes a significant negative factor, and this is one reason why magnetic targeting carrier is still far from satisfactory. Compared with intravenous injection, the artery injection has more advantages, since the magnetic carriers have more chances to access to the target site, avoid clearance by RES, and then stopped by external magnetic filed.[2–4]

The term "biocompatibility" encompasses many different properties of the materials, however, two important aspects of the biomaterial screening refer to their *in vitro* cytotoxicity and blood compatibility behavior.[11] The cell lines of mouse fibroblasts (L929) and mouse macrophages (RAW264.7) were widely used in biocompatibility studies. L929 was recommended by many standard institutions as reference cell line for the cytotoxicity testing of polymers[12,13] and RAW264.7 was used for uptake iron oxide nanoparticles.[14]

In this study, we evaluated the magnetic targeting of SPION-alginate with the magnetic field both *in vitro* and *in vivo*. Biocompatibility of SPION-alginate was measured by hemolysis assay and erythrocytes aggregation assay, and *in vitro* cytotoxicity of L929 cells and RAW264.7 cells. Meanwhile, the labeling of RAW264.7 cells with SPION-alginate was examined.

MATERIALS AND METHODS

Chemicals and magnetic field

The SPION-alginate was a kind of superparamagnetic iron oxide nanoparticles stabilized by alginate macromolecules with good stability and good magnetism.[10] The SPION-alginate was prepared by a modified two-step coprecipitation method. The ferric and ferrous chlorides (molar ratio of 2:1.5) were dissolved in distilled water and chemical precipitation was achieved by adding 5 mol/L NaOH solution at 60°C. The sodium alginate solution was added to the suspension and was stirred vigorously for 30 min. The mixture was heated at 80°C with slow stirring for 1 h and then sonicated for 20 min. All the above processes were run under total N_2 protection. The obtained suspension was dialyzed against deionized water. Finally, the suspension was centrifuged at 10,000 rpm for 20 min to remove the solid material, and the black supernatant, namely SPION-alginate, was collected.

The SPION-alginate had a core (iron oxide nanoparticles) diameter of 5–10 nm, a hydrodynamic diameter of 193.8 nm, and ξ-potential of −67.5 mV. Saturation magnetization (Ms) of the SPION-alginate in suspension was 40 emu/g at 27°C. T1 relaxivity and T2 relaxivity in 0.9% NaCl solution determined by a 1.5 T MRI scanner at 20°C were 7.86 ± 0.20 s^{-1} mM^{-1} and 281.2 ± 26.4 s^{-1} mM^{-1}, respectively.[10]

A cuboid permanent neodymium iron boron magnet (NdFeB-permanent magnet) with length, width, and height of 33, 22, and 11 mm, respectively, was purchased from Beijing Sheng Magnetic Science & Tech (Beijing, China). The magnet with the surface magnetic field of 3500 G was used to produce the magnetic field. And all other reagents used were of analytical reagent grade.

Localization of SPION-alginate with magnetic field *in vitro*

The apparatus of localization of SPION-alginate with external magnetic field *in vitro* was shown in Figure 1. At first, the roller pump was turned on and the rate of distilled water (flow medium) was set to 8 mL/min and 0.5 mL SPION-alginate of 6.04 mg Fe/mL was injected at

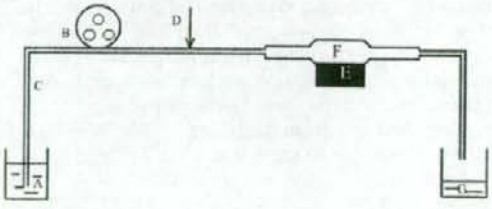

Figure 1. The *in vitro* apparatus of location of SPION-alginate with the external magnetic field. (A) flow medium (distilled water, 8 mL/min); (B) roller pump; (C) rubber tube; (D) injection site of SPION-alginate; (E) magnet; (F) glass tube; (G) eluted medium.

the injection part in the rubber tube. At 10 min after circulation, the glass tube with magnet was erected gently to pour the iron oxide particles unlocated tightly. The remnants of SPION-alginate in the glass tube captured by the magnet were separated, and 6M HCl solution was added to dissolve the iron oxide nanoparticles. The iron content was measured by *o*-phenanthroline method.[15] The ratio of iron content captured by the magnet to injected one was referred to as localization ratio *in vitro*. The experiment was repeated in triplicate.

Magnetic targeting evaluation *in vivo*

Male Sprague–Dawley rats weighing 250 ± 20 g were purchased from Department of Laboratory Animal Science of Peking University Health Science Center. NIH guidelines for the care and use of laboratory animals (NIH Publication #85-23 Rev. 1985) have been observed. Rats were divided into two groups randomly. One group was operated with magnetic field at the right thigh. Before the magnetic targeting of SPION-alginate was carried out, rats were anesthetized by intraperitoneal injection of 1.5 g/kg of ethyl carbamate. The right thigh was disinfected with iodine tincture and 70% alcohol by turns, 30,000 IU penicillin was given by intramuscular injection, and the femoral artery was separated. The SPION-alginate at a dose of 12 mg Fe/kg body weight was injected into the femoral artery at the right thigh under the magnetic field. When the magnetic targeting was performed, the distance between the magnet and the target site was 3 mm, the magnetic field intensity at the target site was 3000 G determined by Gaussmeter, and the magnetic field gradient was 2000 G/cm. The magnetization of SPION-alginate in suspension under the applied magnetic field of 3000 G was 36 emu/g.

After the magnetic targeting, rats were sacrificed by being cut abdominal aorta. The right thigh with magnetic field was referred to as the target site and the left thigh without magnetic field was referred to as the nontarget site in this paper. The right thigh (the target site), left thigh (the nontarget site), liver, and spleen of rats were immediately collected and frozen at −20°C until analysis. Concerning the thigh of rat, the leg was cut from inguinal groove to knee joint to get thigh part, and the thigh was decorticated, followed by removing the bone, separating the muscle of the thigh. Another group was operated without magnetic field at the right thigh, and other conditions were the same as the group with magnetic filed. The iron content in the right thigh, the left thigh, liver, and spleen were determined as follows. The tissues were digested in a beaker with the mixture acid of HNO_3-$HClO_4$ (4:1 v:v) for 48 h at room temperature, and then the solution was evaporated to dryness in sand bath at 100°C. Finally 37.5% HCl was added to the beaker to dissolve the solid and the iron content was determined by *o*-phenanthroline method. The ratio of iron content retained at the right thigh to that of injected was regarded as the localization ratio *in vivo*.

After the magnetic targeting, some of the right thigh (the target site) was intersected, embedded in 4% paraformaldehyde solution (pH 7.4), and then observed at light microscopy after Perls staining and hematoxylin and eosin (H&E) staining.

Ten hours after SPION-alginate application with or without magnetic field on the right thigh, magnetic resonance imaging (MRI) was performed on a 3.0 T clinical MR scanner (GE HD, Milwaukee, WI) with a GPFLEX coil. T2*-weighted gradient recalled echo (GRE) sequence with a coronary plane was used for imaging with the following parameters: repetition time (TR) of 460 ms; echo time (TE) of 6.6 ms; flip angle of 25°; bandwith of 62.5 kHz; field of view of 10 × 10 cm, slice thickness of 3 mm with no gap; matrix of 256 × 128.

Hemolysis assay *in vitro*

A hemolysis test was performed following the procedure reported previously.[16] The rabbit erythrocyte suspension in 0.9% NaCl (2% (v/v)) was prepared. The SPION-alginate of different concentrations, 0.9% NaCl solution (negative control group as 0% hemolysis) or distilled water (positive control group as 100% hemolysis) was added to the erythrocyte suspension and they were incubated for 3 h at 37°C. After centrifugation at 4000 rpm for 10 min, the absorbance of the supernatant was determined at 540 nm to evaluate the leakage of hemoglobin. Percentage of hemolysis was calculated by $(A_S - A_N - A_{SB})/(A_P - A_N) \times 100\%$, where A_S was the average absorbance of the SPION-alginate in erythrocyte suspension, A_N was the average absorbance of 0.9% NaCl solution in erythrocyte suspension (0% hemolysis), A_P was the average absorbance of distilled water in erythrocyte suspension (100% hemolysis). Because the SPION-alginate still had some extent absorbance at 540 nm after centrifugation, so the average absorbance of SPION-alginate only in 0.9% NaCl solution (A_{SB}) is introduced to the equation in order to eliminate the effect of SPION-alginate itself. The experiment was done in triplicate.

Erythrocytes aggregation assay

Rabbit erythrocytes suspension 200 μL was mixed with the indicated amount of SPION-alginate and incubated for 1 h at 37°C in a 24-well plate. The plate was examined by an inverted microscope (Leica DMIRE2, Germany).

Cell culture

L929 cells and RAW264.7 cells were cultured in RPMI 1640 medium (Gibco-Invitrogen, NY) supplemented with 10% (v/v) heat-inactivated newborn calf serum (NCS) (Hyclone, USA), 200 U/mL penicillin, 100 U/mL streptomycin, and 0.11 mg/mL sodium pyruvate. Cells were all maintained in a 5% CO_2 atmosphere at 37°C.

In vitro cytotoxicity evaluation

To determine cytotoxicity, a 3-(4,5-dimethylthiazol-2-yl)-2,5-diphenyl tetrazolium bromide (MTT) assay was performed.[17] The cells were plated at a density of 5×10^4 cells/well for RAW264.7 and 3×10^4 cells/well for L929 in 96-well plate and cultured for 24 h at 37°C in a 5% CO_2 atmosphere. For cytotoxicity without NCS, the medium in

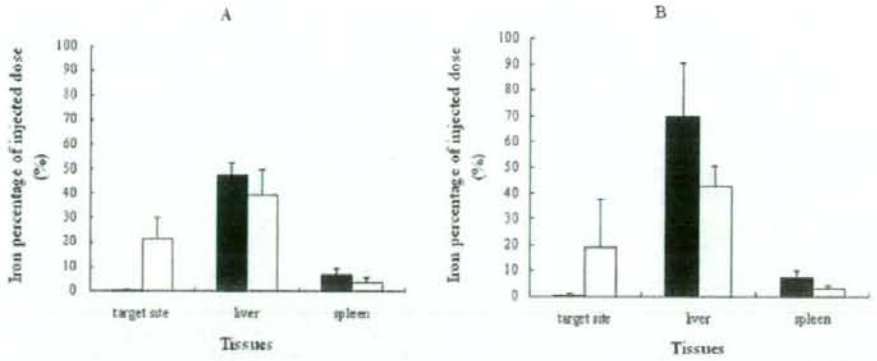

Figure 2. The iron percentage of injected SPION-alginate in target site, liver, and spleen with (□) or without (■) 3500 G magnetic field at 0.5 h (A) or 2 h (B) after femoral arterial injection of SPION-alginate at a dose of 12 mg Fe/kg. Data represent mean ± SD ($n = 3$).

the wells was replaced with 90 μL RPMI 1640 medium, 24 h later, 10 μL serial dilutions of the SPION-alginate were added to cells for 24 h with final iron concentrations from 6.25 to 100.0 μg/mL, and 10 μL RPMI 1640 medium was added to cells as control sample. For cytotoxicity with NCS, the medium in the wells was replaced with 90 μL RPMI 1640 medium with 10% NCS and 10 μL serial dilutions of SPION-alginate were added with the same iron concentrations as mentioned earlier for 24 h. The cells were washed once with phosphate-buffered saline (PBS, pH 7.4) and replenished with 100 μL medium, and then 10 μL MTT solution (Sigma, USA) at 5 mg/mL in saline solution was added to each well. After 4 h of incubation, the medium was removed and formazan crystals were solubilized with dimethylsulphoxide (DMSO) for 10 min at room temperature. The absorbance of each well was then measured on a microplate reader (Bio-Rad Model 550, USA) at a wavelength of 570 nm, with 655 nm as a reference wavelength. The relative cell viability (%) related to control wells was calculated by $(A_{test}/A_{control}) \times 100\%$. where A_{test} was the absorbance of the test sample and $A_{control}$ was the absorbance of control sample. The experiments were run in hexakis and were repeated three times.

Cell labeling with SPION-alginate

RAW264.7 cells were seeded at a density of 5×10^4 cells/mL in 35-mm culture plate at 37°C in a 5% CO_2 atmosphere. After 24 h, the SPION-alginate was added to cells with final iron cation concentrations ranging from 12.5 to 50.0 μg/mL for various incubation times (1–24 h). And then the cells were washed with PBS to remove excess SPION-alginate. For Prussian blue staining, which indicated the presence of iron, the cells were fixed with 4% glutaraldehyde (Merck, Germany) for 10 min and were washed with PBS, followed by incubation with 2% potassium ferrocyanide in 6% HCl for 30 min. After the wash, they were counterstained with nuclear fast red for 5 min.[18] The specimens were then examined under a light microscope (Olympus BH2, Japan).

RESULTS

Localization of SPION-alginate with magnetic field *in vitro*

From the iron content of SPION-alginate captured by the magnet, the localization ratio *in vitro* was (56 ± 5.1)% ($n = 3$).

Magnetic targeting evaluations *in vivo*

Figure 2 showed the iron accumulation in target site, liver and spleen with or without magnetic field via femoral artery injection of SPION-alginate at a dose of 12 mg Fe/kg. At 0.5 h [Fig. 2(A)] and 2 h [Fig. 2(B)] after injection, the localization ratios *in vivo* were about 20%, the iron contents in the right thigh (the target site) with magnetic field were significantly higher than those in the left thigh without magnetic field, and at the same time, the iron contents in liver and spleen with magnetic field were lower than those without magnetic field. The results suggested that the SPION-alginate had some magnetic targeting effect *in vivo*.

In Figure 3, the ratios of iron content (right thigh/left thigh) at 0.5 and 2 h after injection were 1.17 and 1.33 without magnetic field, indicated the SPION-alginate did not be detained in injection site. On the contrary, the ratios of iron content at 0.5 and 2 h after injection were 8.88 and 7.50 with magnetic field, showed the SPION-alginate could be retained at target site with the magnetic field.

With magnetic field at 0.5 h, the femoral artery was filled with iron oxide while the femoral vein was not [Fig. 4(A)], providing a visual evidence for the magnet localization ability of SPION-alginate. Without magnetic field at 0.5 h, the iron oxide was not found

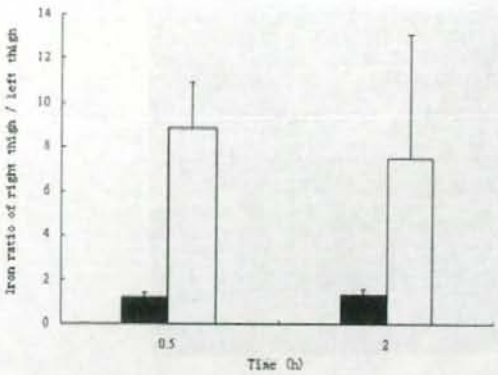

Figure 3. Iron ratio of right thigh (target site) and left thigh (nontarget site) with (□) or without (■) magnetic field at 0.5 and 2 h after injection of SPION-alginate. Data represent mean ± SD ($n = 3$).

both in femoral artery and in femoral vein [Fig. 4(B)], suggesting that no SPION-alginate was detained in the vascular system without magnetic field.

Iron oxide is well-known to significantly shorten the transverse relaxation times (T2 or T2*) with a subsequent loss of MR signal intensity.[19] Therefore, iron oxide can result in a strong decrease in signal intensity (negative enhancement) of the tissues where they accumulate. Figure 5(A) on T2*-weighted image showed the localization of the iron oxide nanoparticles at the right thigh (circle) with the magnetic field, but no localization was showed without magnetic field [Fig. 5(B)].

Hemolysis and erythrocytes aggregation analysis

The leakage of hemoglobin was used to quantify the erythrocytes damage by the SPION-alginate. As shown in Table I, the hemolysis of three preparations of SPION-alginate with different series concentrations were below 5%. So the SPION-alginate did not show hemolytic effect, that is no destruction to the red blood cell membranes. Furthermore, erythrocytes were incubated with the SPION-alginate for 1 h at 37°C, and no aggregation was observed.

Cytotoxicity analysis

The results of the MTT assay indicated that the viability of L929 and RAW264.7 apparently unaltered

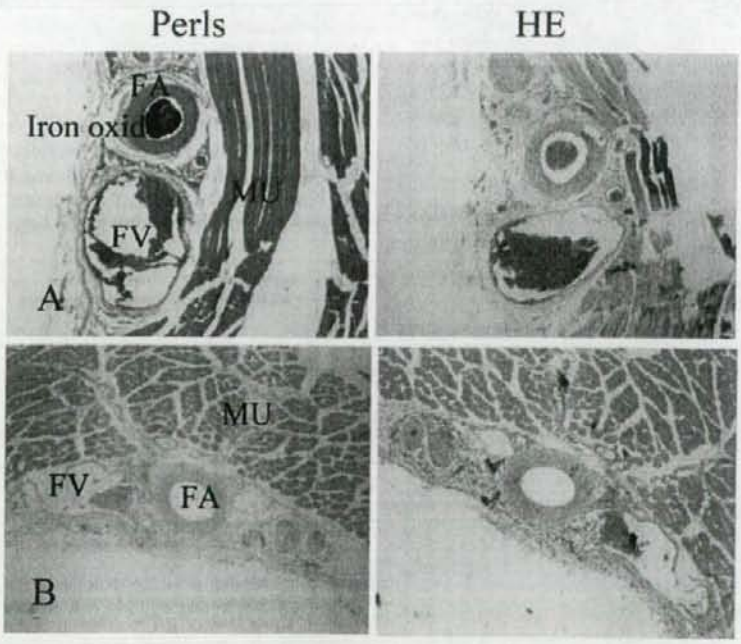

Figure 4. Micrographs of rat right thigh (target site) after femoral arterial injection with magnetic field (A) or without magnetic field (B) at 0.5 h. The tissues were stained with H&E and Perls. FA, femoral artery; FV, femoral vein; MU, muscle (×40 magnification). [Color figure can be viewed in the online issue, which is available at www.interscience.wiley.com.]

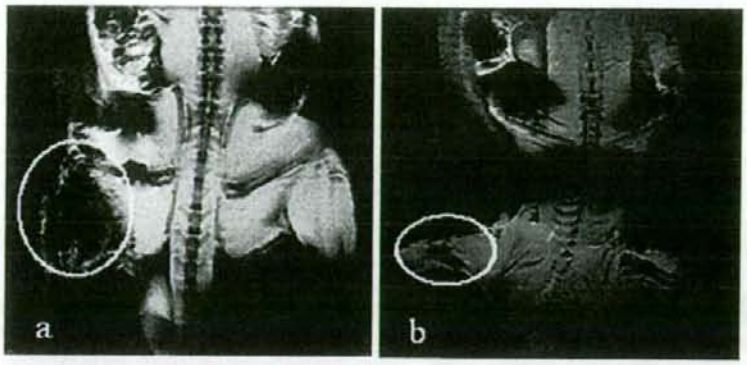

Figure 5. T2*-weighted MRI of right thigh after femoral injection of SPION-alginate with 0.5 h exposure time to magnetic field (A) or not (B). The images were taken at 10 h after injection, which still showed accumulation of iron oxide in target site with the magnetic field, since the strong signal intensity decreased (white circle in A). But the iron oxide did not accumulate in target site (white circle in B), which could be attributed to the slight change of signal intensity without the magnetic field.

upon exposure to various concentrations of SPION-alginate for 24 h with or without NCS (Fig. 6).

Cell labeling with SPION-alginate

Following 1–24 h incubation with SPION-alginate, almost all RAW264.7 cell labeling were achieved. It was evident that the labeled RAW264.7 cells contained abundant Fe_3O_4 nanoparticles in the cytoplasm after incubation with the iron concentration of 12.5, 25.0, and 50.0 μg/mL. The SPION-alginate was internalized into RAW264.7 cells in a concentration- and time- dependent manner (Fig. 7). At a concentration of 25.0 μg/mL, cells started to internalize iron particles already after 1 h incubation [Fig. 7(B)] and the internalization was increased from 1 to 24 h incubation [Fig. 7(C–E)]. For 5 h of incubation at different concentrations, it showed the amount of Prussian blue positive particles in cytoplasma as follow: 50.0 > 25.0 > 12.5 μg/mL. However, no stainable iron was detected in the control cells [Fig. 7(A)].

TABLE I
Hemolysis Percentage of Rabbit Erythrocytes at 37°C After 3 h Incubation With Different Concentrations of SPION-Alginate

SPION-Alginate Concentration (mg Fe/mL)		
Bulk Suspension	Final Suspension	Hemolysis (%)
2.08	0.04	−0.34 ± 0.16
2.08	0.08	0.71 ± 0.78
2.08	0.12	0.29 ± 0.16
2.08	0.17	1.15 ± 0.34
2.08	0.21	2.08 ± 1.48
3.62	0.07	0.23 ± 1.15
3.62	0.14	0.62 ± 1.41
3.62	0.22	1.03 ± 0.70
3.62	0.29	3.19 ± 1.56
3.62	0.36	3.19 ± 1.09
5.74	0.11	1.38 ± 0.96
5.74	0.23	0.62 ± 0.53
5.74	0.34	2.21 ± 0.89
5.74	0.46	2.35 ± 1.74
5.74	0.57	3.24 ± 0.26

Data represent mean ± SD (n = 3). The hemolysis >5% was regarded as erythrocytes hemolysis.

DISCUSSION

To optimize magnetic targeting, several factors need to be considered, (a) the magnetic field, including magnetic intensity and magnetic intensity gradient, should be of sufficient strength to attract the magnetic nanoparticles into the target site; (b) the

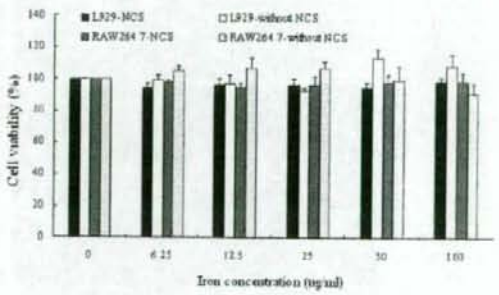

Figure 6. Viability of L929 cells and RAW264.7 cells exposed to SPION-alginate for 24 h at various iron concentrations ranging from 6.125 to 100.0 μg/mL. Cell viability is expressed as the mean ± SD of the percentage of absorbance of controls, where 100% equals viability of the control cells. The experiments were performed in hexakis and were repeated three times.

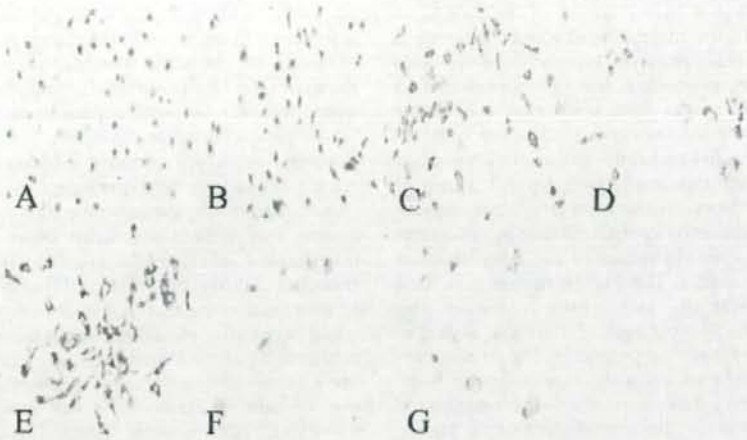

Figure 7. Photomicrographs of Prussian blue stained labeled and control RAW264.7 cells. Cells were cultured with different concentrations of SPION-alginate and harvested after different incubation times. Note the abundant iron particles in the cytoplasm of the cells (blue dots). (A) control; (B) SPION-alginate 25.0 μg/mL, 1 h; (C) SPION-alginate 25.0 μg/mL, 5 h; (D) SPION-alginate 25.0 μg/mL, 12 h; (E) SPION-alginte 25.0 μg/mL, 24 h; (F) SPION-alginate 12.5 μg/mL, 5 h; (G) SPION-alginate 50.0 μg/mL, 5 h (×400 magnification). [Color figure can be viewed in the online issue, which is available at www.interscience.wiley.com.]

magnetic particles should be of a suitable size with good magnetization and biocompatibility; (c) the method of injection should have good access to the target site and the particles should avoid clearance by RES.

In the magnetic targeting study, we employed three methods: iron content measurement, histological evaluation, and MRI. The SPION-alginate could be retained in the target site under the magnetic field with the localization ratio of 56% *in vitro* and the localization ratio of 20% *in vivo*, while reducing accumulation in the liver and spleen (Fig. 2). In addition, without magnetic field, the SPION-alginate would not be retained at the injection site (Fig. 4). The localization ratio .of SPION-alginate *in vivo* was lower than that *in vitro* under the same magnetic field. One of the most important factors affecting the localization ratio of SPION-alginate *in vivo* was the rapid blood flow rate approximately 30 cm/s in large arteries.[20] Hence, part of the SPION-alginate would be flushed by the high blood flow rate which caused the decrease of the localization ratio *in vivo*. In addition, the SPION-alginate was still be phagocytosed by RES although by the artery administration.

Without magnetic field, the accumulation of SPION-alginate in liver (47.54%) and in spleen (6.66%) by femoral artery administration at 0.5 h was significantly lower than that in liver (>80%) and in spleen (10%) by vein administration at 0.5 h (data were not shown), which proved that artery injection was more advantageous than vein injection when the SPION-alginate was targeted to the sites other than liver and spleen. Furthermore, it was reported that intravenous infusion of magnetic drug particles was ineffective to make tumor remission, but the combination of artery infusion with a magnetic field was safe and effective.[2] At present, intraarterial injection of chemotherapeutic agents is approved and well accepted for treatment of liver metastases, and it has occasionally been used for other tumor types such as inoperable head and neck tumors.[21] Many other studies also confirmed the efficacy of arterial administration of magnetic targeting.[3,4,22,23] Currently, the doxorubicin hydrochloride absorbed to magnetic targeted carriers (MTC-DOX) is under clinical investigation for the treatment of patients with primary hepatocellular carcinoma (HCC). It was reported that the particles could be retained at HCC under the applied magnetic field after 28 days by intraarterial administration in human clinical trials.[21] Furthermore, a multicenter, phase I/II trial of hepatic intraarterial deliver of MTC-DOX in patients with HCC and a phase I/II dose escalation study of MTC-DOX in patients with metastatic liver tumors have been undertaken, the results indicated that MTC-DOX could be localized regionally following intraarterial administration without clinically significant toxicities in all cases.[4,23]

The magnetization of the particles was related to the magnetic field strength and the magnetic field gradient. The higher magnetic flux density and magnetic gradient it is, the better the location effect is.[2] Until now, the maximum magnetic field reported was a magnetic flux density of a maximum of 1.7

and 1.0 T at 10 mm below the tip of the pole shoe produced by electric magnet[2] and a remanence field of 1.3 T by NdFeB-permanent magnet.[24] In previous studies, it was suggested that a magnetic field strength of 0.8 T was sufficient to exceed linear blood flow in the intratumoral vasculature.[20] However, a magnetic field of only 250–1000 G has been used to locate the iron oxide particles (0.5–5 μm) in liver and lung.[25] One of the most important reasons for the great difference in strength of magnetic field used above was the difference of the magnetization of iron oxide particles. The high magnetic flux density focused onto the target area is one of the obstacles for effectively targeting. The use of larger particles, as previously suggested by Lübbe and Bergemann,[26] and the use of a stronger magnetic field, are the two approaches to overcome this problem. If the magnetization of the particle is low, a higher magnetic field is needed and vice versa. Therefore, the selection of magnetic field depends on the magnetization of the magnetic carrier. NdFeB-permanent magnet with the surface magnetic field of 3500 G and with the magnetic gradient of 2000 G/cm was used in this study. We achieved a high concentration of iron oxide within the target site after femoral artery administration of the SPION-alginate, which was seen by quantitative evaluation of iron (Figs. 2 and 3), histological (Fig. 4) and MRI (Fig. 5) methods.

As respect to the time of magnetic field added, the shortest time reported was 15 min and the longest time was 24 h.[22,24] In this study, the SPION-alginate had some magnetic targeting effect under the magnetic field at 0.5 h and as the time was prolonged to 2 h, it did not produce better magnetic target. It might be explained that the iron oxide of strong magnetism would soon be absorbed under the magnetic field of 3500 G, while those of poor magnetism would not be absorbed as the time increased and could still be phagocytosed by RES. We speculate that the time of magnetic field added depends both on the magnetization of the particles and the intensity of magnetic field. The higher magnetization of particles and the higher intensity of magnetic field, the shorter time of magnetic field.

Concerning magnetic targeting, there are many practical applications of the magnetic nanoparticles, such as magnetic drug targeting,[2–5,20,23,24] magnetic fluid hyperthermia,[6] and MRI.[9,19] The magnetic nanoparticles can act as carriers of drug and gene for site-specific drug and gene delivery. For example, the SPION-alginate can be functionalized with specific drug like chemotherapeutic drugs for chemical therapy or radioactive isotope for radionuclide therapy. Another promising application of the magnetic nanoparticles is magnetic fluid hyperthermia as one of cancer therapy strategies. When the magnetic carrier is localized at the target site with the applied magnetic field, some heat is generated under an alternating magnetic field due to magnetic hysteresis of magnetic particles. Furthermore, the magnetic nanoparticles can result in a strong decrease in MR signal intensity (negative enhancement) of the tissues where they accumulate. Therefore, it will play an important role in MR contrast imaging to better discriminate healthy and pathological tissues.

Although some encouraging data were achieved in this study, there are many issues to be further investigated on magnetic targeting. For example, a potential complication that could arise with the use of ferrofluid is the fact that an embolization process could occur after magnetic targeting, and the embolization is to some extent favorable for cancer treatment because of their cut-off of the blood and nutrition of tumor.[8] However, it was reported that the therapeutic effect resulted from the action of the chemotherapeutic agent itself, rather than intratumoral embolization by the particles.[2] On the other hand, the localization accuracy of the particles at the target site needs to be optimized, and the design of the magnetic field with greater magnetic field intensity and magnetic field gradient is quite important and needs to be improved.

Compared with the corresponding control cells, no significant change was observed in the viability of RAW264.7 cells and L929 cells with various different concentrations of SPION-alginate for 24 h incubation with or without serum (Fig. 6). Hence, we considered that the SPION-alginate was not toxic to RAW264.7 cells and L929 cells. In addition, the SPION-alginate did not induce erythrocytes hemolysis and erythrocytes aggregation. Accordingly, the SPION-alginate was generally considered to be of good biocompatibility.

Figure 7 showed that the labeled RAW264.7 cells contained abundant Fe_3O_4 nanoparticles in the cytoplasm after 1–24 h incubation with the various concentrations of SPION-alginate. The high RAW264.7 labeling efficiency with the SPION-alginate seems to be related firstly to the nonspecific process of nanoparticles adsorption on the cell membrane in the form of clusters, secondly to their subsequent internalization into endosomes, as introduced by other authors.[14,27] The interaction of the SPION-alginate with living cells should be further investigated. Moreover, the Fe_3O_4 nanoparticles bound to alginate macromolecule strands like "fruit" in the "tree," not simply coated by the polymer. They were visually confirmed by atomic force microscopy.[10] It is indicated that alginate would not hamper their interactions with cell membrane, which could be caused by steric coating effect. Besides, the good bioadhesion property of alginate is beneficial to the adsorption of SPION-alginate on the cell membrane. Because of the nonspecific cellular uptake mediated by adsorptive

endocytosis, the SPION-alginate labeling may be nonspecific and potentially applicable to a wide variety of cells, making it useful for cellular imaging strategies.

CONCLUSIONS

With magnetic field, the SPION-alginate had a localization ratio of 56% *in vitro* and 20% *in vivo*, meanwhile, the contents of the SPION-alginate in liver and spleen were reduced. The magnetic targeting effect was established by evaluating the iron content ratio of target site/nontarget site, and was visually confirmed by histological evaluation and MRI. Furthermore, the SPION-alginate was considered to be biocompatible in respects of cytotoxicity and hemolysis.

References

1. Häfeli UO. Magnetically modulated therapeutic systems. Int J Pharm 2004;277:19–24.
2. Alexiou C, Arnold W, Klein RJ, Parak FG, Hulin P, Bergemann C, Erhardt W, Wagenpfeil S, Lübbe AS. Locoregional cancer treatment with magnetic drug targeting. Cancer Res 2000;60:6641–6648.
3. Leakakos T, Ji C, Lawson G, Peterson C, Goodwin S. Intravesical administration of doxorubicin to swine bladder using magnetically targeted carriers. Cancer Chemother Pharmacol 2003;51:445–450.
4. Just R, Hoh C, Vogl T, Neese P, Doemeny J, Schechter M, Varney R, Stanton W, Schiemann M, Goldfarb P. A phase I/II single arm trial to determine the safety, tolerability, and biological activity of intrahepatic delivery of doxorubicin hydrochloride adsorbed to magnetic targeted carriers (MTX-DOX) in patients with metastatic tumors in the liver. Eur J Cancer Suppl 2003;1:S292–S293.
5. Häfeli U, Pauer G, Failing S, Tapolsky G. Radiolabeling of magnetic particles with rhenium-188 for cancer therapy. J Magn Magn Mater 2001;225:73–78.
6. Jordan A, Scholz R, Maier-Hauff K, Johannsen M, Wust P, Nadobny J, Schirra H, Schmidt H, Deger S, Loening S, Lanksch W, Felix R. Presentation of a new magnetic field therapy system for the treatment of human solid tumors with magnetic fluid hyperthermia. J Magn Magn Mater 2001;225:118–126.
7. Scherer F, Anton M, Schillinger U, Henke J, Bergemann C, Krüger A, Gänsbacher B, Plank C. Magnetofection: Enhancing and targeting gene delivery by magnetic force in vitro and in vivo. Gene Ther 2002;9:102–109.
8. Widder KJ, Senyei AE, Scarpelli GD. Magnetic microspheres: A model system for site specific drug delivery in vivo. Proc Soc Exp Biol Med 1978;158:141–146.
9. Wang YX, Hussain SM, Krestin GP. Superparamagnetic iron oxide contrast agents: Physicochemical characteristics and applications in MR imaging. Eur Radiol 2001;11:2319–2331.
10. Ma HL, Qi XR, Maitani Y, Nagai T. Preparation and characterization of superparamagnetic iron oxide nanoparticles stabilized by alginate. Int J Pharm 2007;333:177–186.
11. Sgouras D, Duncan R. Methods for the evaluation of biocompatibility of soluble synthetic polymers which have potential for biomedical use: 1-Use of the tetrazolium-based colorimetric assay (MTT) as a preliminary screen for evaluation of in vitro cytotoxicity. J Mater Sci: Mater Med 1990;1:61–68.
12. Biological Evaluation for Medical Devices, Part 5: Tests for Cytotoxicity: In Vitro Methods. United States Pharmacopeia XXIII, 1995.
13. Biological Evaluation of Medical Devices, Part 5: Test for In Vitro Cytotoxicity. ISO 10993-5 (EN 30993-5), 1999.
14. Wilhelm C, Billotey C, Roger J, Pons JN, Bacri JC, Gazeau F. Intracellular uptake of anionic superparamagnetic nanoparticles as a function of their surface coating. Biomaterials 2003;24:1001–1011.
15. Hagar W, Vichinsky EP, Theil EC. Liver ferritin subunit ratios in neonatal hemochromatosis. Pediatr Hematol Oncol 2003;20:229–235.
16. Regulations of new drug license application in China.State Food and Drug Administration in China; 1999. p 24.
17. Mosmann T. Rapid colorimetric assay for cellular growth and survival: Application to proliferation and cytotoxicity assays. J Immunol Methods 1983;65:55–63.
18. Arbab AS, Bashaw LA, Miller BR, Jordan EK, Lewis BK, Kalish H, Frank JA. Characterization of biophysical and metabolic properties of cells labeled with superparamagnetic iron oxide nanoparticles and transfection agent for cellular MR imaging. Radiology 2003;229:838–846.
19. Saini S, Stark DD, Hahn PF, Wittenberg J, Brady TJ, Ferrucci JT. Ferrite particles: A superparamagnetic MR contrast agent for the reticuloendothelial system. Radiology 1987;162:211–216.
20. Senyei A, Widder K, Czerlinski C. Magnetic guidance of drug carrying microspheres. J Appl Phys 1978;49:3578–3583.
21. Link KH, Kornmann M, Formenti A, Leder G, Sunelaitis E, Schatz M, Pressmar J, Beger HG. Regional chemotherapy of non-resectable liver metastases from colorectal cancer-literature and institutional review. Langenbecks Arch Surg 1999;384:344–353.
22. Rudge S, Peterson C, Vessely C, Koda J, Stevens S, Catterall L. Adsorption and desorption of chemotherapeutic drugs from a magnetically targeted carrier (MTC). J Control Release 2001;74:335–340.
23. Koda J, Venook A, Walser E, Goodwin S. A multicenter, phase I/II trial of hepatic intra-arterial delivery of doxorubicin hydrochloride adsorbed to magnetic targeted carriers in patients with hepatocellular carcinoma. Eur J Cancer 2002;38(Suppl 7):S18.
24. Schulze K, Koch A, Schöpf B, Petri A, Steitz B, Chastellain M, Hofmann M, Hofmann H, von Rechenberg B. Intraarticular application of superparamagnetic nanoparticles and their uptake by synovial membrane—An experimental study in sheep. J Magn Mag Mater 2005;293:419–432.
25. Goodwin S, Peterson C, Hoh C, Bittner C. Targeting and retention of magnetic targeted carriers (MTCs) enhancing intra-arterial chemotherapy. J Magn Mag Mater 1999;194:132–139.
26. Lübbe AS, Bergemann C.Selected preclinical and first clinical experiences with magnetically targeted 4'-epidoxorubicin in patients with advanced solid tumors. In: Häfeli U, Schütt W, Teller J, Zborowski M, editors. Scientific and Clinical Application of Magnetic Carriers. New York:Plenum; 1997. p 457–480.
27. Wilhelm C, Gazeau F, Roger J, Pons JN, Bacri JC. Interaction of anionic superparamagnetic nanoparticles with cells: Kinetic analyses of membrane adsorption and subsequent internalization. Langmuir 2002;18:8148–8155.

Available online at www.sciencedirect.com

ScienceDirect

International Journal of Pharmaceutics 354 (2008) 217–226

INTERNATIONAL JOURNAL OF PHARMACEUTICS

www.elsevier.com/locate/ijpharm

Pharmaceutical Nanotechnology

Superparamagnetic iron oxide nanoparticles stabilized by alginate: Pharmacokinetics, tissue distribution, and applications in detecting liver cancers

Hui Li Ma[a], Yu Feng Xu[b], Xian Rong Qi[a,*], Yoshie Maitani[c], Tsuneji Nagai[d]

[a] *Department of Pharmaceutics, School of Pharmaceutical Sciences, Peking University, Beijing 100083, China*
[b] *Department of Radiology, First Hospital, Peking University, Beijing 100034, China*
[c] *Institute of Medicinal Chemistry, Hoshi University, Shinagawa-Ku, Tokyo 142-8501, Japan*
[d] *The Nagai Foundation Tokyo, Hon-Komagome, Bunkyo-ku, Tokyo 113-0021, Japan*

Received 13 August 2007; received in revised form 18 November 2007; accepted 20 November 2007
Available online 28 November 2007

Abstract

The objectives of this study were to describe the pharmacokinetics and tissue distribution of superparamagnetic iron oxide nanoparticle (SPIO) stabilized with alginate (SPIO-alginate), and investigate its potential in detecting liver cancers as a newly developed magnetic resonance (MR) contrast agent. Pharmacokinetics and tissue distribution of SPIO-alginate were investigated in Sprague–Dawley rats. The results showed that SPIO-alginate was eliminated rapidly from serum with the half-life of 0.27 h at 109.5 μmol Fe/kg and accumulated dominantly in liver and spleen with a total percentage of more than 90% of dose after intravenous injection. The studies of pharmacokinetics and distribution of SPIO-alginate in rats indicated the MR contrast agent, based on SPIO, mainly accumulating in targeting organs that contain phagocytosing cells, i.e. liver and spleen. The efficacies in detecting hepatocellular carcinoma (HCC) of rat with primary liver cancer and xenograft liver cancers of rabbit were investigated before and after injection of SPIO-alginate. The signal intensity of liver parenchyma in rabbit with VX2 tumor after injection of SPIO-alginate was reduced sharply resulting in a significant contrast between liver parenchyma and tumor. Detection of the HCC in rat model was also demonstrated. The present study provides evidence that SPIO-alginate might have the ability to improve the detection of liver tumors as an MR contrast agent, and the efficacy is associated with the SPIO specifically located in Kupffer cells in hepatic sinusoid.

Keywords: Superparamagnetic iron oxide nanoparticles (SPIO); Pharmacokinetics; Distribution; Liver cancers; Contrast agent; Alginate

1. Introduction

MR imaging is one of the most useful non-invasive methods in the field of diagnostic imaging, which is characterized by its high resolution of soft-tissues and by its non-exposure to radiation. To better differentiate healthy and pathological tissues, paramagnetic gadolinium based contrast agents which shorten the longitudinal relaxation time (T1) and increase the contrast of the image (positive enhancement) are mainly used today (Weinmann et al., 2003). Compared to gadolinium based contrast agents, SPIO can produce enhanced relaxation rates in specific organs at lower dose than paramagnetic ions, because of their larger magnetic moment (Corot et al., 2006; Wang et al., 2001). Generally speaking, the transverse relaxation (T2 and T2*) effect of SPIO is mostly utilized in detection of liver lesions by MR imaging. SPIO are distributed in reticuloendothelial cells, such as Kupffer cells (KCs), according to phagocytic activity, and cause local field inhomogeneities that produce rapid dephasing of neighboring proton spins, resulting in a shortening of T2 relaxation times. In contrast, liver tumors such as metastatic liver cancer and HCC cannot absorb these agents because of the lack of reticuloendothelial cells. Therefore, the contrast between tumor tissue and surrounding normal liver tissue is enhanced because of signal loss in the liver tissue (Saini et al., 1987). Hence, SPIO can produce a strong decrease in MR signal intensity (negative enhancement) in the tissues where they accumulate, such as the liver, spleen, bone marrow, and lymph node (Saini et al., 1987; Corot et al., 2006).

* Corresponding author. Tel.: +86 10 82801584; fax: +86 10 82802791.
E-mail address: qixr2001@yahoo.com.cn (X.R. Qi).

0378-5173/$ – see front matter © 2007 Elsevier B.V. All rights reserved.
doi:10.1016/j.ijpharm.2007.11.036

Until now, two SPIO preparations have already been approved for clinical use, especially for liver MR imaging, such as Ferumoxides (i.e. Endorem® in Europe, Feridex® in the USA and Japan, Advanced Magnetics, USA) coated with dextran (Weissleder et al., 1989), and Ferucarbutran (i.e. Resovist® in Europe and Japan, Schering, Germany) coated with carboxydextran (Reimer et al., 1995). Furthermore, several SPIO preparations have been investigated in human for imaging applications, such as VSOP-C184, a very small SPIO coated with citrate (Taupitz et al., 2004), and Feruglose (Clariscan; Amersham Health, Oslo, Norway) where iron oxide particles have been stabilized with oxidized starch that consist of carbohydrate-polyethylene glycol (Kellar et al., 2000).

In our previous work, SPIO stabilized with alginate (SPIO-alginate) have been successfully prepared (Ma et al., 2007) and the SPIO-alginate have good biocompatibility and some magnetic targeting under the magnetic field (Ma et al., 2007a). As the coating material of iron oxide, alginate is known for binding many multivalent ions *in vitro* such as Ca^{2+}, Ba^{2+}, Fe^{2+}, and Fe^{3+}. The high stability of SPIO-alginate is probably caused by the binding of the carboxyl group of alginate to iron oxide nuclei (Ma et al., 2007). It was reported that the absorption of Fe, Cr, and Co was significantly reduced after oral administration of sodium alginate in rats, while Ca and Zn absorption was not affected (Harmut-Hoene and Schelenz, 1980). Hence, it is necessary to investigate the effect of alginate and SPIO-alginate on the iron level *in vivo*, even if some COO^- terminals of alginate have been bound to iron oxide in SPIO-alginate.

We presumed that using SPIO-alginate as an intravenous contrast medium, detection of malignant liver lesions by MR imaging might be improved. Once iron oxide particles are taken up by the macrophages situated in the liver of reticuloendothelial system (RES) but not by tumor cells, the contrast between liver parenchyma and liver lesion would significantly increase, which is caused by the distinct signal loss in liver parenchyma and the almost stable signal intensity in malignant liver tumors (Saini et al., 1987; Clement et al., 1991; Nakayama et al., 1998; Imai et al., 2000; Bourrinet et al., 2006).

To investigate whether this highly stabilized SPIO-alginate is a kind of ideal MR contrast for liver imaging, the pharmacokinetics and tissue distribution of SPIO-alginate in rats were first examined in this study. After that, the efficacy of SPIO-alginate for the detection of liver cancers was evaluated in two kinds of tumor models, VX2 liver tumor in rabbit and primary liver cancer in rat.

2. Materials and methods

2.1. Contrast agent

Typical iron oxide nanoparticles were Fe_3O_4 with a core diameter of 5–10 nm. Meanwhile, SPIO-alginate had a hydrodynamic diameter of 193.8 nm with good stability as well as superparamagnetism, and its ξ-potential was −65.0 mV. T1 and T2 relaxivities of SPIO-alginate in physiological saline (1.5 T, 20 °C) were 7.86 ± 0.20 and $281.2 \pm 26.4\ s^{-1}\ mM^{-1}$, respectively. Other properties of SPIO-alginate were described in detail in the previous publication (Ma et al., 2007, 2007a). For MR imaging experiment, SPIO-alginate was diluted to a concentration of 8.9 μmol Fe/mL with physiological saline.

2.2. Pharmacokinetics, tissue distribution and histological evaluation in normal rats

Male Sprague–Dawley rats weighing 150 ± 20 g were purchased from Experimental Animal Center of Peking University, China. All care and handling of animals were performed with the approval of Institutional Authority for Laboratory Animal Care of Peking University, which followed the guidelines established by the China Council for Animal Care. The animals were anesthetized by intraperitoneal injection of 1.0 g/kg of ethyl carbamate. The pharmacokinetics studies (using whole blood) were carried out with 29 rats which were divided into four groups randomly. The rats were intravenously injected with the following formulations individually: SPIO-alginate at a dose of 109.5 μmol Fe/kg (SPIO-low dose) ($n = 18$), SPIO-alginate at a dose of 218.9 μmol Fe/kg (SPIO-high dose) ($n = 3$), 1 mL 0.6% (w/v) alginate solution (alginate solution) ($n = 3$), and 1 mL physiological saline (saline) ($n = 5$). About 0.3 mL blood samples were taken by retro-orbital venous plexus puncture at 0 min (before intravenous injection), 5 min, 10 min, 30 min, 1 h, 3 h, 6 h, 12 h, 24 h, 48 h, 96 h, 168 h, and 336 h after injection, respectively.

The pharmacokinetics studies (using serum) were obtained in rats by quantitative determination of iron in serum. Twenty rats were divided into four groups ($n = 5$ per group) in random and injected with SPIO-low dose, SPIO-high dose, alginate solution, and saline, respectively. About 0.6 mL blood samples were collected from retro-orbital venous plexus puncture at 0 min, 5 min, 10 min, 30 min, 1 h, 3 h, 6 h, 12 h, and 24 h after injection, respectively. Then each clotted blood sample was centrifuged at 7000 rpm for 20 min to get serum sample.

The basic serum iron concentration was calculated from the average serum iron concentration at 0 min of all the rats. The serum iron concentrations at various time points after administration were calculated by subtracting the basic serum iron concentration. Serum iron concentration–time profiles were analyzed by WinNonlin computer software, Version 3.1 (Pharsight Corporation, Mountain View, CA), using noncompartmental method with bolus intravenously administration. The following parameters were obtained: maximum tissue concentration (C_{max}), elimination rate constant (λ), elimination half-life ($T_{1/2}$), area under the curve (AUC), and mean residence time (MRT).

The tissue distribution of SPIO-alginate at a dose of 109.5 μmol Fe/kg in rats (total 21) were studied at 0, 0.5, 3, 24, 48, 96, and 336 h after injection, which was performed simultaneously with the blood pharmacokinetics study of SPIO-low dose. Tissues of interest (blood, liver, spleen, heart, lungs, and kidneys) were collected immediately at various time points, weighted, and frozen at −20 °C until analysis.

Liver and spleen concentration-time profiles were analyzed by WinNonlin computer software using a noncompartmental method with a single extravascular dosing. The iron concentrations in liver and spleen at various time points were calculated

by subtracting the iron concentration in liver or in spleen at 0 h (before injection), respectively. The following parameters were obtained: time of maximum concentration (T_{max}), C_{max}, λ, $T_{1/2}$, AUC, and MRT.

Liver and spleen were removed at 0.5, 24, 96, and 336 h after injection of SPIO-low dose, and at 336 h after injection of SPIO-high dose and alginate solution, respectively. Then the samples were fixed in 4% paraformaldehyde solution (pH 7.4) for hematoxylin-eosin (HE) staining and Perls staining. The liver and spleen section specimens were examined under a light microscopy after staining.

2.3. Iron content measurement

For quantitative determination of iron content, blood, serum and tissue samples were digested in a beaker with the mixed acid of HNO_3–$HClO_4$ (4:1, v:v) for 48 h at room temperature, and then evaporated to dryness at 100 °C by sand bath with electric hot plate. Finally 37.5% HCl solution was added to the beaker to dissolve the solid and the iron content was determined by *o*-phenanthroline method (Hagar et al., 2003).

2.4. Tumor models of rats and rabbits

Male Sprague–Dawley rats (130–140 g, total 35) were used. The model of primary liver cancer in rats ($n = 29$) was established by giving 70 mg diethylnitrosoamine (DENA, Sigma–Aldrich, USA) per kg weight 14 times at 7-d intervals through intragastric administration with physiological saline. As DENA was sensitive to light, a fresh solution was prepared for each administration and kept in dark bottles for short periods. The rats of control group ($n = 6$) were raised in the normal condition.

VX2 rabbit tumor was cut into small pieces (about 1 mm^3), and then implanted into left hepatic lobe to establish single liver cancer in rabbit. After implantation, VX2 tumor rapidly developed in the liver and the implanted tumor formation was detected by computed tomography (CT) on week 2. The surgery and implantation procedures have been described in detail in the previous publication (Hauff et al., 1997).

2.5. MR imaging in normal rat

All MR imaging examinations were performed by using a clinical 3.0 T MR scanner (Signa Horizon, General Electric Medical Systems, Milwaukee, WI) with a surface coil. For the investigations of liver enhancement in normal rats, the normal rats ($n = 6$) were imaged before and after injection of SPIO-alginate at a dose of 20 μmol Fe/kg through femoral vein. T1-weighted fast spin echo (FSE) or spoiled gradient-recalled (SPGR) sequence, T2-weighted fast recovery fast spin echo (FRFSE) sequence, and T2*-weighted gradient-recalled echo (GRE) sequence were used for the MR imaging. All the sequences were applied with a bandwidth of 31.25 kHz and slice thickness of 3 mm. Other parameters were as follows: T1-weighted FSE sequence (TE 14.6 ms; TR 800 ms; Echo train length 3; Matrix 288 × 192; NEX 4; FOV 8 × 8); T1-weighted SPGR sequence (TE 3.7 ms; TR 100 ms; Flip angles 60°; Matrix 128 × 128; NEX 6; FOV 8 × 4); T2-weighted FRFSE sequence (TE 150 ms; TR 3000 ms; Echo train length 21; Matrix 128 × 128; NEX 6; FOV 8 × 5.6); T2*-weighted GRE sequence (TE 4.7 ms; TR 300 ms; Flip angles 15°; Matrix 128 × 128; NEX 6; FOV 8 × 4).

2.6. MR imaging in tumor animals and histological evaluation

For rabbits with VX2 tumor, unenhanced and enhanced T2*-weighted images were investigated before and after injection of SPIO-alginate at a dose of 20 μmol Fe/kg using SPGR sequence with the following parameters: TR of 220 ms, TE of 5.2 ms, flip angles of 70°, slice thickness of 4 mm, slice gap of 1.0 mm, matrix of 512 × 160, field of view of 13 × 13, and bandwidth of 62.5 kHz.

For rats with primary liver cancer, unenhanced and enhanced images were obtained before and after injection of SPIO-alginate at a dose of 20 μmol Fe/kg using T2*-weighted GRE sequence with the parameters just mentioned above in MR imaging for normal rats. The rats were sacrificed within 2–12 h after MR imaging evaluation. Then, liver specimens were fixed, the size, number, and shape of the lesions were observed, and the lesions were histologically identified after HE staining and Perls staining. The pathological changes e.g. hyperplastic nodules, cirrhotic and HCC, were also observed.

2.7. Imaging analysis

Quantitative analysis was performed by using an operator defined region of interest (ROI) of 6 mm^2 on T1-weighted, T2-weighted and T2*-weighted images, respectively. Major vessels were avoided when the signal intensities of liver parenchyma and tumor were measured. Measurements included signal intensity (SI) of the HCC (SI_{HCC}), the liver parenchyma without cirrhosis (SI_{liver}), the liver parenchyma with cirrhosis ($SI_{cirrhosis}$), and standard deviation of noise ($S.D._{noise}$), respectively. Signal-to-noise ratio (SNR) was then calculated on both pre- and post-SPIO-alginate images by taking the SI_{HCC}, SI_{liver} or $SI_{cirrhosis}$ dividing by each $S.D._{noise}$. In addition, contrast-to-noise ratio (CNR) was calculated with the following formula: $(SI_{HCC} - SI_{cirrhosis})/S.D._{noise}$, and the relative contrast was expressed as $SI_{HCC}/SI_{cirrhosis}$.

3. Results

3.1. Pharmacokinetics of SPIO-alginate in normal rats

After injection of SPIO-alginate at both low dose and high dose, the blood iron concentration first gradually decreased from the maximal concentration at 0.083 h to the lowest concentration at 48 h (from 515.5 to 266.3 μg/mL for SPIO-low dose group, and from 647.7 to 333.6 μg/mL for SPIO-high dose group, respectively), and then recovered to the initial concentration before injection (about 471.9 μg/mL) at 96 h. In addition, the blood iron concentration after injection of alginate solution and saline also showed the similar profile (mildly down and up), and

Table 1
Serum iron concentration in rats after intravenous injection of SPIO-low dose (109.5 μmol Fe/kg), SPIO-high dose (218.9 μmol Fe/kg), 1 mL 0.6% (w/v) alginate solution, and saline. The basic serum iron concentration before administration was 10.64 ± 4.58 μg/mL. Data represent mean ± S.D.

Time (h)	SPIO-low dose	SPIO-high dose	Alginate solution	Saline
0	9.32 ± 5.55	9.08 ± 3.42	10.96 ± 4.73	21.09 ± 6.13
0.083	143.75 ± 18.61	356.10 ± 42.82	6.16 ± 1.52	15.75 ± 3.71
0.167	131.90 ± 13.56	310.44 ± 64.55	5.48 ± 0.57	15.01 ± 1.18
0.5	57.62 ± 19.43	183.87 ± 37.37	7.49 ± 0.88	17.23 ± 2.23
1	19.57 ± 10.82	108.28 ± 38.23	8.52 ± 3.07	10.80 ± 1.88
3	8.74 ± 5.29	19.83 ± 15.31	6.86 ± 2.08	12.51 ± 5.25
6	6.79 ± 3.20	8.68 ± 5.36	4.72 ± 1.61	9.71 ± 0.92
12	3.28 ± 1.01	3.89 ± 2.13	6.96 ± 3.54	6.48 ± 1.23
24	4.52 ± 1.43	3.01 ± 1.75	5.07 ± 1.29	ND

ND: not determined.

the blood iron concentrations in all rats were even under the initial concentration before injection between 6 and 48 h after injection.

The basic serum iron concentration before administration fluctuated between 6.06 and 15.22 μg/mL. The serum iron concentrations at various time points after injection of alginate solution and saline located in the range of basic serum iron concentration (Table 1). But, the serum iron concentrations increased significantly after SPIO-alginate injection and then decreased to the basic serum iron concentration range at 3 h for low dose and at 6 h for high dose. The $T_{1/2}$ of SPIO-alginate was 0.27 ± 0.06 h at low dose and 0.65 ± 0.22 h at high dose calculated by noncompartmental analysis (Table 2).

3.2. Tissue distribution of SPIO-alginate in normal rats

Table 3 showed that the iron concentrations in liver and spleen significantly increased, while those in blood, lungs, heart, and kidneys slightly changed after injection of SPIO-alginate at low dose. Considering the weights of organs, the results revealed that more than 80% of the injected iron accumulated into the liver, and about 10% into the spleen while less than 2% was found in the kidneys, heart and lungs, respectively. The iron concentrations in the liver and the spleen were high between 0.5 and 24 h, and began to decrease after 24 h. The tissue distribution parameters in liver and spleen for SPIO-alginate in rat calculated by the WinNonlin program using noncompartmental model was given in Table 2. It indicated that the elimination of iron in liver was slower than that in spleen.

3.3. Histological evaluation in normal rat

Although the experiments were carried out at different time points before and after injection of SPIO-alginate as described in methods, only the typical micrographs were shown in order to shorten the length of writing. HE staining could reflect the effect of SPIO-alginate on the morphology of tissues. The sections indicated that there was no significant change on the basic structure of all the specimens of liver and spleen, though there was a little edema of hepatocytes in the perimeter section of liver lobules (Fig. 1).

Perls staining was performed to detect the iron particles dyed blue. Stainable iron was observed in KCs in hepatic sinusoid, in splenic cord of the perimeter section of follicle and in splenic red pulp at 0.5, 24, 96, and 336 h after injection of low dose of SPIO-alginate (Fig. 1). Additionally, iron particles were distributed in the perimeter section of liver lobules at 0.5 h and in the center section at 96 h. The amount of iron oxide particles in liver qualitatively peaked between 0.5 and 24 h after injection, and small amounts of particles were still present at 336 h after injection. The results in the spleen were similar to those in the liver.

Table 2
Serum, liver and spleen parameters of SPIO-alginate in rats following intravenous injection at 109.5 and 218.9 μmol Fe/kg using noncompartmental analysis with bolus IV administration for serum and extravascular administration for liver and spleen

Parameters	Serum ($n = 5$)		Liver	Spleen
	Low dose	High dose	Low dose	Low dose
T_{max} (h)	0.083	0.083, 0.176	0.5	24
C_{max} (μg/mL or g)	147.91 ± 20.72	348.99 ± 43.78*	176.64	290.06
λ (h^{-1})[a]	2.95 ± 0.87	1.28 ± 0.40*	0.005	0.0085
$AUC_{0\to 24h}$ (h μg/mL or h μg/g)[b]	68.37 ± 18.87	321.74 ± 123.72*	35,176.83	26,307.97
$T_{1/2}$ (h)	0.25 ± 0.06	0.59 ± 0.20*	139.19	81.98
$MRT_{0\to 24h}$ (h)	0.32 ± 0.11	0.76 ± 0.27*	181.179	86.235

Each value of serum parameter represents the mean ± S.D.
[a] $T_{1/2}$ was calculated from the terminal slope by means of log-linear regression.
[b] AUC was calculated by linear trapezoidal rule.
* $P < 0.05$, compared with the value of low dose in serum.

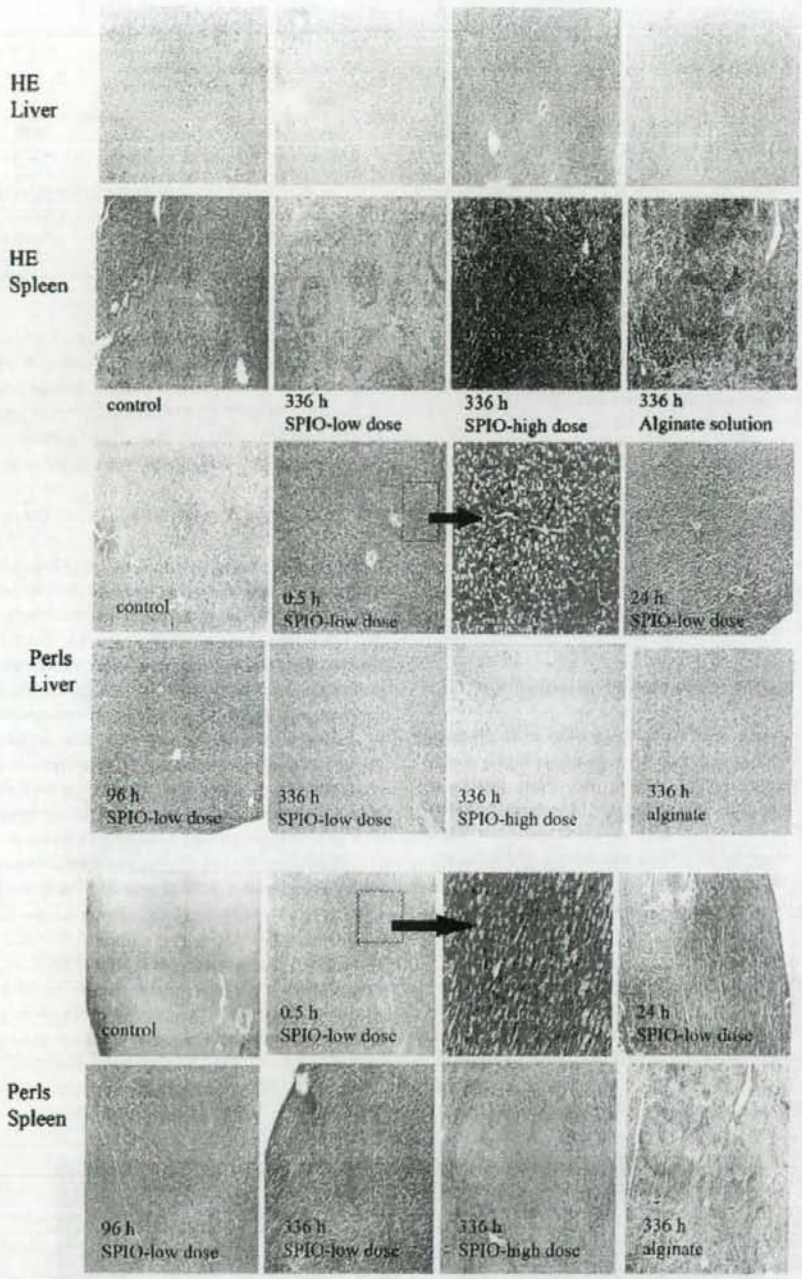

Fig. 1. Sections of liver and spleen of normal rat with HE staining and Perls staining (magnification ×10).

Table 3
Iron concentration in different tissues at different timepoints after intravenous injection of SPIO-low dose (109.5 μmol Fe/kg). Data represent mean ± S.D. ($n = 3$)

Time (h)	Iron concentrations in tissue (μg Fe/mL in whole blood; μg Fe/kg in heart, liver, spleen, lung, and kidney)					
	Whole blood	Liver	Spleen	Lung	Kidney	Heart
0	471.93 ± 55.06	58.42 ± 7.56	112.22 ± 24.69	56.67 ± 9.54	52.01 ± 8.61	59.61 ± 13.38
0.5	439.31 ± 54.98	235.05 ± 19.62	350.46 ± 51.17	60.20 ± 14.84	47.23 ± 9.95	59.56 ± 7.07
3	342.28 ± 68.38	199.22 ± 19.69	353.72 ± 144.36	55.40 ± 11.95	41.93 ± 3.73	66.03 ± 19.40
24	313.44 ± 113.85	226.57 ± 38.78	402.28 ± 187.31	79.25 ± 10.67	48.64 ± 9.36	51.28 ± 4.48
48	266.34 ± 27.49	191.45 ± 33.44	247.70 ± 18.61	71.47 ± 13.58	45.96 ± 4.06	58.56 ± 5.04
96	402.88 ± 96.96	159.99 ± 9.16	176.21 ± 27.11	63.05 ± 1.98	44.29 ± 4.87	51.87 ± 5.37
336	552.05 ± 36.63	89.76	122.68	45.45	55.24	40.08

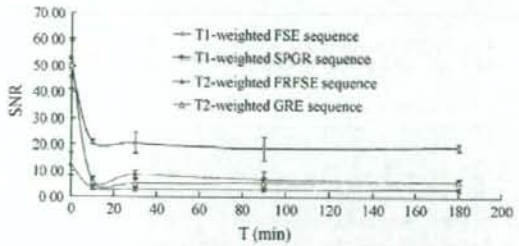

Fig. 2. *In vivo* SNR of liver in normal rats after injection of SPIO-alginate at a dose of 20 μmol Fe/kg. A negative enhancement was observed with T1-weighted, T2-weighted, and T2*-weighted sequences.

3.4. Liver enhancement of SPIO-alginate in normal rat

Fig. 2 showed the liver SNR before and after SPIO-alginate injection on both T1-weighted and T2-weighted images. Compared with unenhanced images ($t = 0$), the SNR decreased at 10 min on T1-weighted FSE images, T1-weighted SPGR images, T2-weighted FRFSE images, and T2*-weighted GRE images, after SPIO-alginate injection, and remained almost stable up to 180 min, respectively. Hence, a remarkable negative enhancement was immediately obtained after the injection of SPIO-alginate.

3.5. MR imaging for rabbit tumor model

Fig. 3 showed the MR signal intensity of liver parenchyma (thick arrow) decreased, however, that of the tumor (fine arrow) did not obviously change and the borderline of the tumor was found more clearly in comparison with that of unenhanced image. The photograph and sections of rabbit VX2 tumor with Perls staining after MR imaging enhanced with SPIO-alginate were shown in Fig. 4. It was evident that there was a single tumor in the liver with the size of about 2.5 cm in accordance with that in MR images in Fig. 3. Iron oxide particles were observed in the normal part of liver rather than in the tumor (Fig. 4).

3.6. MR imaging for rats with primary liver cancer

During the process of establishing primary liver cancer model of rats, eight rats were dead because of hemorrhage in the tumor and poor resistance. In addition, two rats were chosen randomly and identified as cirrhosis at 12 weeks, and four rats were identified as HCC with cirrhosis at 15 weeks from MR imaging and pathological evaluation. Fifteen rats survived at 18 weeks in MR imaging experiment. All the fifteen rats were accompanied with severe cirrhosis, and no HCC was found in any rat on MR images before the injection of SPIO-alginate (pre-SPIO, unenhanced imaging). However, 22 HCCs were found in 11 rats after injection of SPIO-alginate (post-SPIO, enhanced imaging) and four rats were diagnosed as simple cirrhosis even after injection of SPIO-alginate. The SNR_{liver} decreased from 48.95 ± 4.87 at pre-SPIO to 6.43 ± 3.37 at post-SPIO and the $SNR_{cirrhosis}$ from 45.51 ± 11.71 to 23.47 ± 7.52. However, the SNR_{HCC} remained almost stable (45.51 ± 11.71 at pre-SPIO and 40.53 ± 12.98 at post-SPIO). Furthermore, the CNR of HCC increased from zero at pre-SPIO to 17.69 ± 3.69 at post-SPIO and the relative contrast increased from 1.0 at pre-SPIO to 1.79 ± 0.31 at post-SPIO. Hence, the contrast between HCC and liver parenchyma was significantly increased and the detection of HCC was improved.

In Fig. 5, compared with the signal intensity on unenhanced T2*-weighted GRE images, the liver signal intensity of nor-

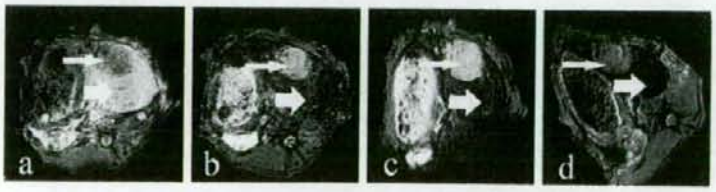

Fig. 3. T2*-weighted FSPGR images (TR/TE, 220 ms/5.2 ms) of xenograft liver cancer in rabbit at (a) 0 min (unenhanced imaging), (b) 10 min, (c) 30 min, and (d) 60 min after intravenous injection of SPIO-alginate at a dose of 20 μmol Fe/kg. After injection of SPIO-alginate, the liver parenchyma (thickness arrow) showed a distinct signal loss, whereas that of the tumor (fine arrow) remained almost unaffected. Hence, the contrast between tumor and liver parenchyma was significantly increased.